Research Article | Vol. 8, No. 3 | 1 Mar 2017 | BIOMEDICAL OPTICS EXPRESS 1466
Biomedical Optics EXPRESS

Persistent luminescence tomography for small animal imaging

XU CAO,[1] YUZHU GONG,[1] YANG LI,[1] SHOUPING ZHU,[1] XUANXUAN ZHANG,[1] YONGHUA ZHAN,[1] FEI KANG,[2] JING WANG,[2] AND JIMIN LIANG[1,*]

[1]*Engineering Research Center of Molecular and Neuro Imaging of the Ministry of Education & School of Life Science and Technology, Xidian University, Xi'an, Shaanxi 710071, China*
[2]*Department of Nuclear Medicine, Xijing Hospital, Fourth Military Medical University, Xi'an, China*
[*]*jimleung@mail.xidian.edu.cn*

Abstract: Fluorescence imaging is a widely used *in vivo* optical imaging technique for preclinical studies, but strong tissue autofluorescence and external excitation light make it suffer from a low signal-to-noise ratio (SNR). Recently, a new optical imaging method using persistent luminescence has become of interest due to its advantage of circumvention of autofluorescence and bleed-through of excitation light during signal acquisition. In this work, we proposed a tomographic imaging method based on persistent luminescence named persistent luminescence tomography (PLT), which can obtain three dimensional distributions of persistent luminescence probes deep inside small animals. Persistent luminescence signals can last several hours after excitation, which makes it possible for PLT to collect signals without interference by autofluorescence and bleed-through of excitation light, and then to reconstruct tomographic images of high quality. Phantom and mouse experiments are implemented to verify the feasiblity of PLT.

OCIS codes: (170.3880) Medical and biological imaging; (170.3010) Image reconstruction techniques; (170.6960) Tomography.

References and links

1. T. F. Massoud and S. S. Gambhir, "Molecular imaging in living subjects: seeing fundamental biological processes in a new light," Genes Dev. **17**(5), 545–580 (2003).
2. J. K. Willmann, N. van Bruggen, L. M. Dinkelborg, and S. S. Gambhir, "Molecular imaging in drug development," Nat. Rev. Drug Discov. **7**(7), 591–607 (2008).
3. V. Ntziachristos, J. Ripoll, L. V. Wang, and R. Weissleder, "Looking and listening to light: the evolution of whole-body photonic imaging," Nat. Biotechnol. **23**(3), 313–320 (2005).
4. J. V. Frangioni, "Self-illuminating quantum dots light the way," Nat. Biotechnol. **24**(3), 326–328 (2006).
5. T. Matsuzawa, Y. Aoki, N. Takeuchi, and Y. Murayama, "A new long phosphorescent phosphor with high brightness, SrAl2O4:Eu2+,Dy3+," J. Electrochem. Soc. **143**(8), 2670–2673 (1996).
6. T. Aitasalo, P. Deren, J. Hölsä, H. Jungner, J. C. Krupa, M. Lastusaari, J. Legendziewicz, J. Niittykoski, and W. Strek, "Persistent luminescence phenomena in materials doped with rare earth ions," J. Solid State Chem. **171**(1–2), 114–122 (2003).
7. Z. Pan, Y. Y. Lu, and F. Liu, "Sunlight-activated long-persistent luminescence in the near-infrared from Cr3+-doped zinc gallogermanates," Nat. Mater. **11**(1), 58–63 (2011).
8. Q. le Masne de Chermont, C. Chanéac, J. Seguin, F. Pellé, S. Maîtrejean, J. P. Jolivet, D. Gourier, M. Bessodes, and D. Scherman, "Nanoprobes with near-infrared persistent luminescence for in vivo imaging," Proc. Natl. Acad. Sci. U.S.A. **104**(22), 9266–9271 (2007).
9. T. Maldiney, C. Richard, J. Seguin, N. Wattier, M. Bessodes, and D. Scherman, "Effect of core diameter, surface coating, and PEG chain length on the biodistribution of persistent luminescence nanoparticles in mice," ACS Nano **5**(2), 854–862 (2011).
10. A. Abdukayum, J. T. Chen, Q. Zhao, and X. P. Yan, "Functional near infrared-emitting Cr3+/Pr3+ co-doped zinc gallogermanate persistent luminescent nanoparticles with superlong afterglow for in vivo targeted bioimaging," J. Am. Chem. Soc. **135**(38), 14125–14133 (2013).
11. T. Maldiney, M. U. Kaikkonen, J. Seguin, Q. le Masne de Chermont, M. Bessodes, K. J. Airenne, S. Ylä-Herttuala, D. Scherman, and C. Richard, "In vitro targeting of avidin-expressing glioma cells with biotinylated persistent luminescence nanoparticles," Bioconjug. Chem. **23**(3), 472–478 (2012).
12. T. Maldiney, A. Bessière, J. Seguin, E. Teston, S. K. Sharma, B. Viana, A. J. Bos, P. Dorenbos, M. Bessodes, D. Gourier, D. Scherman, and C. Richard, "The in vivo activation of persistent nanophosphors for optical imaging of vascularization, tumours and grafted cells," Nat. Mater. **13**(4), 418–426 (2014).

#280234 https://doi.org/10.1364/BOE.8.001466
Journal © 2017 Received 8 Nov 2016; revised 28 Dec 2016; accepted 11 Jan 2017; published 8 Feb 2017

Biomedical Optics EXPRESS

13. B. Y. Wu, H. F. Wang, J. T. Chen, and X. P. Yan, "Fluorescence resonance energy transfer inhibition assay for α-fetoprotein excreted during cancer cell growth using functionalized persistent luminescence nanoparticles," J. Am. Chem. Soc. **133**(4), 686–688 (2011).
14. W. Cong, G. Wang, D. Kumar, Y. Liu, M. Jiang, L. Wang, E. Hoffman, G. McLennan, P. McCray, J. Zabner, and A. Cong, "Practical reconstruction method for bioluminescence tomography," Opt. Express **13**(18), 6756–6771 (2005).
15. S. R. Arridge, M. Schweiger, M. Hiraoka, and D. T. Delpy, "A finite element approach for modeling photon transport in tissue," Med. Phys. **20**(2), 299–309 (1993).
16. A. R. Arridge, "Optical tomography in medical imaging," Inverse Probl. **15**(2), 41–93 (1999).
17. J. Ripoll, V. Ntziachristos, R. Carminati, and M. Nieto-Vesperinas, "Kirchhoff approximation for diffusive waves," Phys. Rev. E Stat. Nonlin. Soft Matter Phys. **64**(5), 051917 (2001).
18. J. A. Tropp and A. C. Gilbert, "Signal recovery from random measurements via orthogonal matching pursuit," IEEE Trans. Inf. Theory **53**(12), 4655–4666 (2007).
19. V. Temlyakov, "Nonlinear methods of approximation," Found. Comput. Math. **3**(1), 33–107 (2003).
20. G. Yan, J. Tian, S. Zhu, Y. Dai, and C. Qin, "Fast cone-beam CT image reconstruction using GPU hardware," J. XRay Sci. Technol. **16**(4), 225–234 (2008).
21. H. Chen, Y. C. Zhang, C. Chen, Z. L. Wang, and N. Yao, "The Research of Solvothermal Method Preparation of $Y_2O_2S:Eu^{3+}_{0.06}$, $Mg^{2+}_{0.04}$,$Ti^{4+}_{0.01}$ Water-Soluble Red Afterglow Materials," Applied Mechanics and Materials **513–517**, 138–142 (2014).

1. Introduction

As a kind of macroscopic optical imaging, fluorescence imaging (FI) is widely used in biomedical research and drug development owing to its advantages of non-invasive, non-radioactive, high-throughput, easy-to-operate, and cost-effective detection [1–3]. Fluorescence acquisition needs external excitation both in a reflection or transillumination mode, which brings strong tissue autofluorescence and external excitation light into desired fluorescent signals, and suffers from a low signal-to-noise ratio (SNR) [4].

Unlike the short lifetime of fluorescence, persistent luminescence (PL) relates to an optical phenomenon in which a kind of particular material can glow for several hours after excitation with ultraviolet or visible light [5]. These PL materials can store excitation energy and then slowly release it by a photonic emission [6, 7]. Using PL materials for imaging, persistent luminescence imaging (PLI) can separate excitation and emission processes, and completely circumvents the strong tissue autofluorescence and external excitation light in signal acquisition. As a result, PLI has the advantage of high SNR and sensitivity for *in vivo* imaging in small animal applications [8]. Due to this excellent characteristic of PLI, PL materials in nanoscale or so-called PL nanoparticles (PLNPs) have also been functionalized to target specific cells and introduced into sensitive biological imaging of tumor-bearing mouse [9–11]. PLI has also been reported in cell tracking, tumor targeting, and vascularization imaging while exhibiting exceptional sensitivity and penetration that far exceed those afforded by FI [12]. Recent developments have also led to the description of PL based Förster resonance energy transfer for imaging cancer cells [13].

Although PLI has a broad application prospect in biological research, this 2-D photographic imaging is incapable of providing depth information of the PL source inside biological tissues due to strong scattering characteristics. So, we propose tomographic PL imaging named persistent luminescence tomography (PLT) in this work. Combined with a diffuse optical model and image reconstruction algorithm, PLT has the ability to reveal 3-D distributions of the PL source deep inside small animal, which makes it possible to be used for detecting *in situ* tumors. Furthermore, PLT can provide higher quality tomographic images due to no interference of strong tissue autofluorescence and external excitation light compared with fluorescence tomography (FT), a type of tomographic imaging for FI. We investigated its feasibility by using physical phantom and mouse models based on homemade optical and computed tomography (CT) imaging systems.

2. Methods

2.1 Forward model

Although PLT contains excitation and emission prosesses, there is no excitation light during detection of PL signals, which is similar to bioluminescence tomography (BLT), another

Biomedical Optics EXPRESS

optical tomography employing luciferase enzymes for in vivo detection of tagged cells in living animals [14]. Furthermore, the used area shape excitation source in this work can sufficiently excite the whole imaged object, and the flux density of the excitation light inside the imaged object is approximately uniform. Thus, only the emission process is considered for PLT, and the forward model of PLT can be described by a diffusion equation in view of accuracy and computation cost [15]

$$\begin{cases} -\nabla\cdot[D_m(r)\nabla\Phi_m(r)]+\mu_{am}(r)\Phi_m(r)=X(r) & r\in\Omega \\ \Phi_m(r)+2AD_m(r)\nabla\Phi_m(r)\cdot\hat{n}=0 & r\in\partial\Omega \end{cases}. \tag{1}$$

where $\Phi_m(r)$ is the flux density of the PL signal, and X denotes the unknown PL yield. μ_{am} is the absorption coefficient, $D_m = 1/[3(\mu_{am}+\mu_{sm}')]$ is the diffusion coefficient, and μ_{sm}' is the reduced scattering coefficient. Ω and $\partial\Omega$ represent the region of the object and its boundary respectively. A is a boundary constant representing the refractive index mismatched between tissues and the surrounding medium [16].

Here a tangential planar approach named Kirchhoff approximation can be used to find an analytical formulation for Green's functions of the diffusion equation [17]. After discretizing the medium into three dimensional grids, Eqs. (1) can be transformed into the following matrix-form equations:

$$WX=\Phi \tag{2}$$

where W is the weight matrix mapping unknown PL yield X into measurable boundary light intensity Φ.

2.2 Reconstruction method

Reconstruction of PLT is to solve Eq. (2), which is an ill-posed problem, due to insufficient measurement compared with the whole solving domain. Considering the sparse characteristic of unknown source X, orthogonal matching pursuits (OMP) can be used to solve Eq. (2), which is a widely used iterative method for sparse recovery based on the Compressed Sensing theory [18]. OMP uses the observation vector $u=W^*\Phi$ as a good local approximation to the unknown fluorescence yield X, and the largest coordinate of the observation vector u in magnitude is chosen as a nonzero coordinate of the unknown source X in each iteration [19]. Based on this similar idea, if the sparsity level of X is N, we can make use of N biggest coordinates of the observation vector u, rather than the largest one, as N nonzero coordinates of unknown source X. Then, we can use the corresponding N columns of W to form a new weight matrix W_N mapping the nonzero solving domain into measurement Φ.

$$W_N X_N=\Phi. \tag{3}$$

Finally, traditional Tikhonov regularization can be used to solve this sub-equation Eq. (3) with a reduced solving domain. The details of this reconstruction method can be described as the following algorithm:

Input: weight matrix W, measurement Φ, sparse level N and regularization parameter α.

Output: unknown fluorescence yield X.

1. Compute observation vector $u=W^*\Phi$ to local approximate X.
2. Choose a set J_N formed by the coordinates of the N biggest observations from u.
3. Build the reduced solving domain problem $W_N X_N=\Phi$ using the N columns of W and N rows of Φ defined in J_N.

Biomedical Optics EXPRESS

4. Solve the reduced solving domain problem $W_N X_N = \Phi$ using Tikhonov regularization $X_N = \left(W_N^{'} W_N + \alpha I\right)^{-1} \left(W_N^{'} \Phi\right)$.

5. Build the final unknown fluorescence yield X by X_N with coordinates in J_N and 0 with coordinates out of J_N.

2.3 The imaging flow

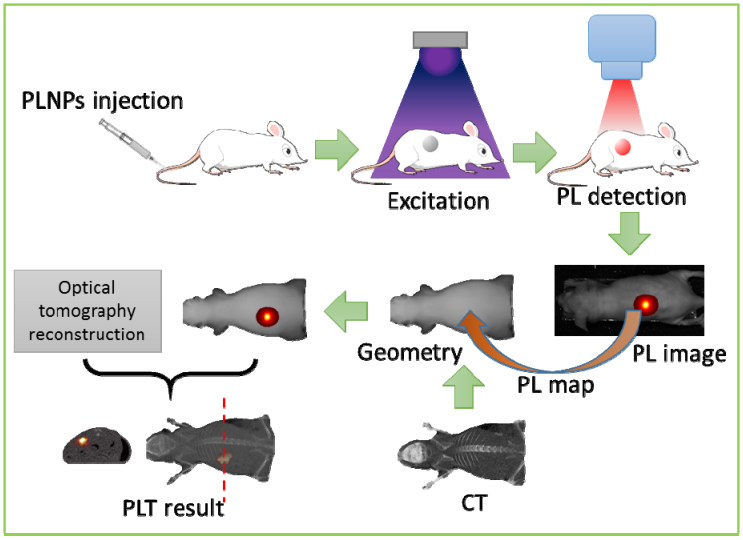

Fig. 1. Flow chart of PLT.

The process of PLT is summarized as Fig. 1. PLNPs are injected into imaged mouse via caudal vein. After arrival at targeted lesions of PLNPs, the imaged mouse is excitated by ultraviolet or visible light for seveal minutes. Then, the PL image can be captured from the top view by an EMCCD camera (iXon DU-897, Andor, U.K.) coupled with a Nikkor 50-mm f/2.8D lens (Nikon, Melville, NY). To acquire the tomographic optical image, the geometry of the imaged mouse is necessary for forward model computation. So, CT scans of the imaged mouse are performed using a homemade CT imaging system, which includes an X-ray tube (Apogee, Oxford Instruments, UK) and a CMOS X-ray detector (C7921, Hamamatsu, Japan). The anatomical structure of the imaged mouse is obtained by using a cone-beam Feldkamp-Davis-Kress (FDK) reconstruction algorithm on the graphics processing unit using an acceleration scheme [20]. PL image is mapped onto the 3-D surface of the imaged mouse, which is extracted from the segmented CT image. Finally, optical forward model computation and image reconstruction are carried out to obtain 3-D distributions of PLNPs inside the imaged mouse.

3. Results

3.1 Comparison between persistent luminescence and fluorescence

To illustrate the advantages that PLI is free from autofluorescence and bleed-through of excitation, a glass cup of 40 mm in height and 20 mm in diameter filled with 1% intralipid solution was employed as a turbid medium. Absorption and reduced scattering coefficients for the medium are 0.002 mm^{-1} of 1 mm^{-1}, respectively, which mimick biological tissues with high absorption and low scattering of light. For fluorescent imaging, a small glass tube filled with 100 uL Cy5.5 NIR dye with a concentration of 0.01 uM was used as the fluorescent target. For PL imaging, a small glass tube filled with 10 mg $Y_2O_2S:Eu^{3+},Ti^{2+}$, and Mg^{4+}, a red

Biomedical Optics EXPRESS

long-lasting PLNPs, was used as the PL target which has characteristic absorption peak in ultraviolet spectrum [21]. Fluorescent and PL targets were fastened to the bottom of the glass cup, and experiments with different depths were implemented by adding different volumes of intralipid solution

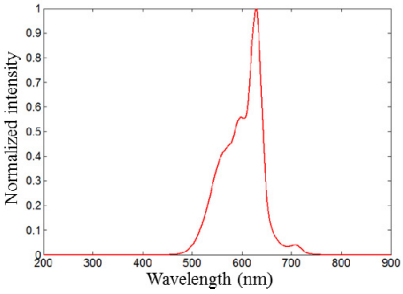

Fig. 2. Emission spectrum of $Y_2O_2S:Eu^{3+},Ti^{2+}$, and Mg^{4+}.

To capture fluorescent images, an area light source was provided by a halogen lamp coupled with an optical fiber and a 640 ± 10 nm bandpass filter to excite the fluorescent target. A 690 ± 20 nm bandpass filter was used to select the fluorescent signals of Cy5.5. The emission spectruman of the PLNPs ranges from 500nm to 720nm with emission peak at 630nm when excited by a 430nm ultraviolet lamp as shown in Fig. 2. Obviously, there is no need to use any filter to capture PLI signals. But to make a fair comparision with FI, the same 690 ± 20 nm bandpass filter was also used to capture PL images after excitation by the ultraviolet lamp about 10 seconds.

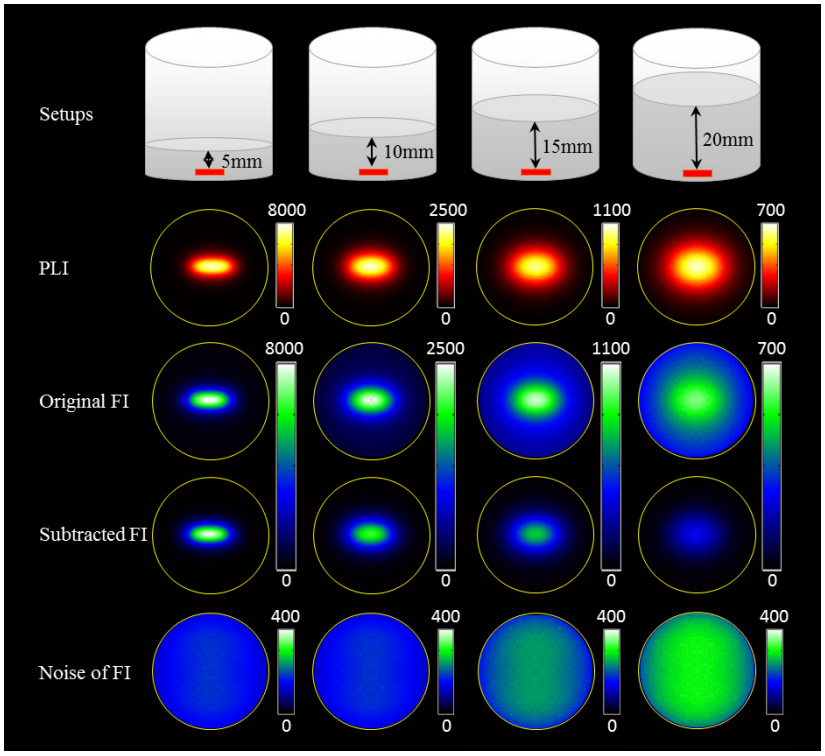

Fig. 3. Image comparisons between PLI and FI. The first row is the setups for different depths. The second row is PLI images for different depths of PLNPs. The last three rows are original FI, subtracted FI and noise of FI images for different depths of fluorescent targets, respectively.

Biomedical Optics EXPRESS

Figure 3 shows PL and the FI images for different depths. The first row is the setups for different depths, and the corresponding PLI and FI images are listed below. Generally, the intensities of PLI and FI images are decreased with depth of intralipid. By adjusting the intensity of exciting light and exposure time for FI acquisition, the maximum of original FI image is almost the same as that of PLI image for each depth. PLI image contains only PLI signals, but original FI image contains not only fluorescent signals but also noises attributed to autofluorescence and bleed-through of excitation light. So the noise of FI image was also acquired by removing fluorescent target with the same acquisition parameters. The intensity for noise of FI image increases slightly with depth of intralipid, that is because a deep one has a high intralipid level and receives strong excitation light when a divergent excitation light source is fixed on the top. The subtracted FI image was obtained by subtracting noise of FI image form original FI image, which contains only FI signals. There is no observable visual difference between original FI image and subtracted FI image, when FI signals are strong enough for 5mm depth case. But original FI images emerge significant visual differences with subtracted FI images when depths are deeper than 5 mm. Besides that, PLI images present similar distributions of optical signals with those of subtracted FI images for all depth cases.

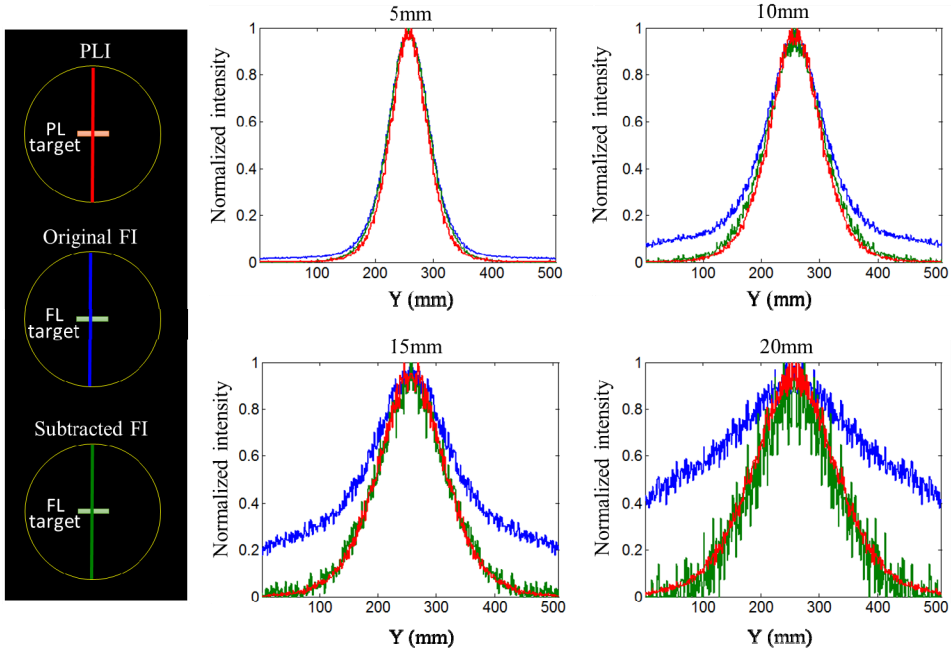

Fig. 4. Resolution comparisons between PLI and FI images. The right profiles of PLI, original and subtracted FI images for different depths were acquired along vertical lines defined in the left diagrams.

Profiles along vertical lines defined on the left of Fig. 4 for PLI, original and subtracted FI images of Fig. 3 are shown on the right of Fig. 4. For PLI, resolution declines only caused by increase of depth, but autofluorescence and bleed-through of excitation light also degrades FI resolution besides depth. After subtracting of noise of FI image, subtracted FI image has the similar profile with PLI image for each depth case.

3.2 Phantom experiments

In the phantom experiment, two polyoxymethylene made semi-cylinders with 20 mm in diameter and 40 mm in height were employed as physical phantoms to mimic biological tissues. Their absorption and scattering coefficients were 0.002 mm^{-1} and 1 mm^{-1} respectively, which was similar to those of biological tissues. Each phantom had a hole drilled

Biomedical Optics EXPRESS

along the axial direction with the depth of 3mm. A small glass tube filled with about 5 mg $Y_2O_2S:Eu^{3+},Ti^{2+}$, Mg^{4+} was used as the PL target, which was inserted into the hole of the phantom to mimic the PLT phantom experiment. After excitation by an ultraviolet lamp for about 10 seconds, we turned off the lamp and captured the PL image with an exposure time of 1s for the CCD camera coupled with a 690 ± 20 nm bandpass filter. Subsequently, micro-CT scans of the phantom were performed (voltage of 50 kVp and current of 1.0 mA for the X-ray source, 360 views with 1° interval). Faltered back-projection (FBP) method was used to reconstruct micro-CT data of the phantom, which were used to supply the geometry of the phantom for forward model calculation of PLT. For comparison, a small glass tube filled with 50 uL Cy5.5 dye with a concentration of 0.01 uM was used as the fluorescent target and inserted into the hole of the phantom to mimic the FT phantom experiment. Original FI image was collected when the phantom was excited by an area light source with a spectrum of 640nm. Then the fluorescent target was removed and the noise of FI image was acquired using the same acquisition parameter. Finnally, a CT image for the FT experiment was obtained with the same setup as PLT experiment.

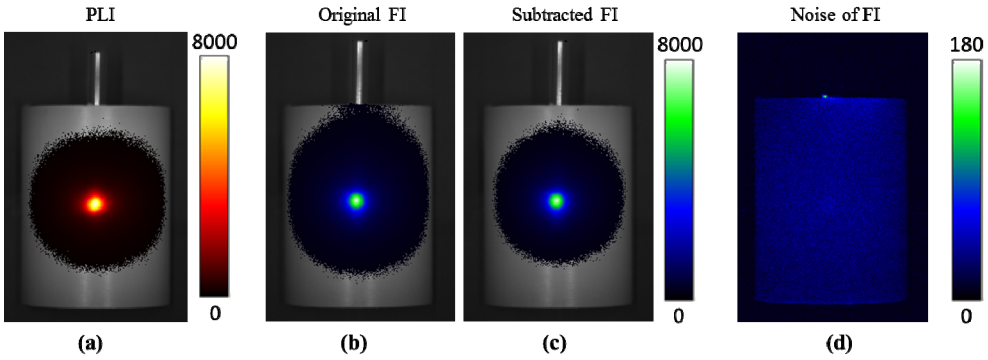

Fig. 5. Comparisons between PLI and FI for phantom experiments. (a) Fused PLI image with the white light image. (b) Fused original FI image with the white light image. (c) Fused subtracted FI image with the white light image. (d) Fused noise of FI image with the white light image.

Without disturbs of autofluorescence, the PL image (Fig. 5(a)) contains only PL signals undergoing scattering and absorbing of the diffused phantom. The original FI image has a slight different distributions of optical signals with those of the PL image, although they contain the same emission spectrum and maximum optical intensity. After removing the noise of FI image from the original FI image, the obtained subtracted FI image has more similar distributions of optical signals with those of PL image, which demenstracts that noises caused by autofluorescence and bleed-through of excitation light can distort true distributions of optical signals.

Biomedical Optics EXPRESS

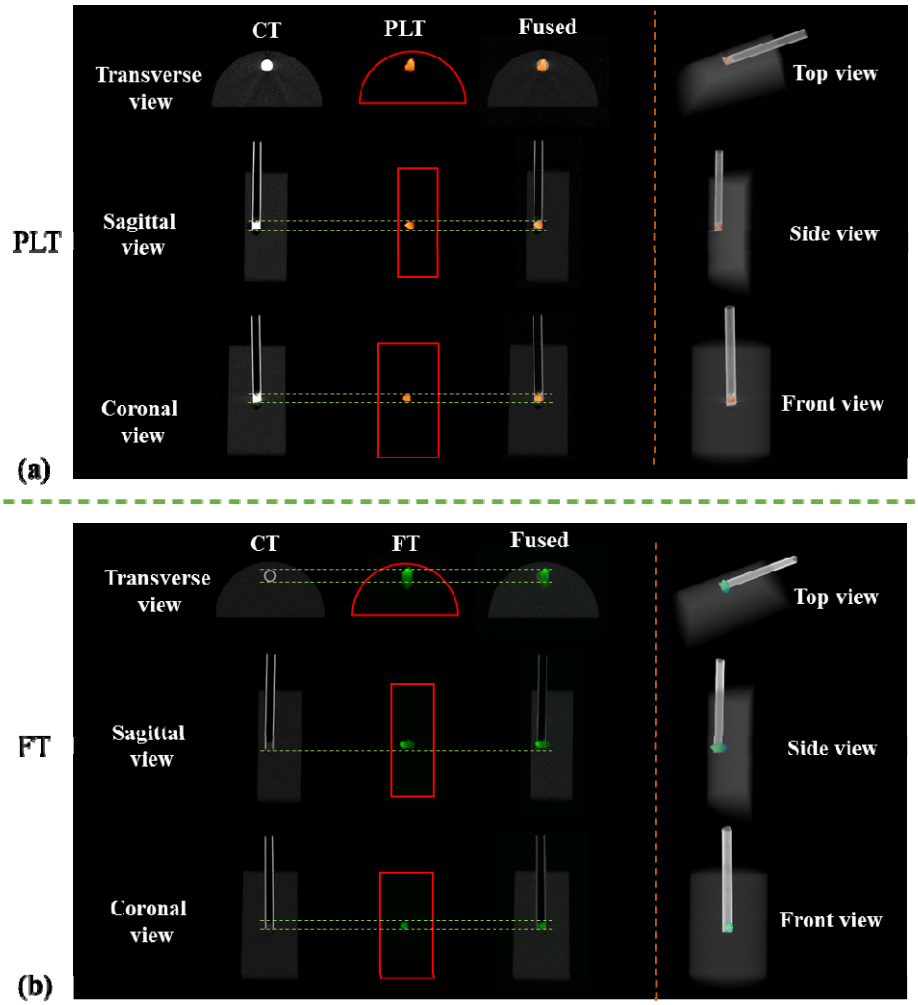

Fig. 6. Reconstructed results for the phantom experiment. (a) 2D sections (left) and 3D renderings (right) fused with CT images for PLT. (b) 2D sections (left) and 3D volume renderings (right) fused with CT images for FT.

Figure 6 shows the reconstructed PLT and FT images, which includes the transverse, sagittal and coronal 2D sections and 3D volume renderings at different viewing angles for PLT and FT reconstructions. The reconstructed PL and fluorescent targets are visually in good agreement with CT images, which can provide their accurate positions. The size of the reconstructed fluorescent target is slightly larger than that of the true one in the CT image. Dice coefficient (DIC) and position (center of gravity) were computed to quantify the reconstructed results as shown in Table 1, and DIC is defined as

$$DIC = 2\frac{|R_R \cap R_s|}{|R_R| + |R_s|}. \quad (4)$$

where *RS* represents the regions of the true target segmented from the CT image, and *RR* represents the regions of the reconstructed target segmented from a reconstructed image. A large DIC means a high agreement of the reconstructed and true targets. For PLT, DIC is 0.66 and position error is 0.39 mm, which is better than FT with DIC 0.52 and position error 0.78 mm.

Biomedical Optics EXPRESS

Table 1. Quantitative analysis for PLT and FT reconstructions of the phantom experiment

	DIC	True position (mm)	Reconstructed position (mm)	Position error (mm)
PLT	0.66	(20.68, 14.30, 33.67)	(20.57, 14.67, 33.71)	0.39
FT	0.52	(20.17, 14.35, 32.70)	(20.80, 14.27, 33.16)	0.78

3.3 Mouse experiments

For mouse experiment, the animal was cared for in accordance with a protocol approved by the Fourth Military Medical University Animal Care and Use Committee. Two nude mice were used as imaged animals. Glass tube containing FI or PL target as the same with the phantom experiment was implanted into rectum by surgical procedure under general anesthesia by intraperitoneal injection of 10% sodium pentobarbital. To avoid traumas of nude mice, the glass tube lubricated with man-rated lubricating oil was gently implanted into rectum with a small entering distance through natural openings of the nude mice. Optical images were captured from a supine position using the similar acquisition processes but with different exposure time for appropriate optical intensities. And then, CT images for PLT and FT were also obtained with the same setup as phantom experiment.

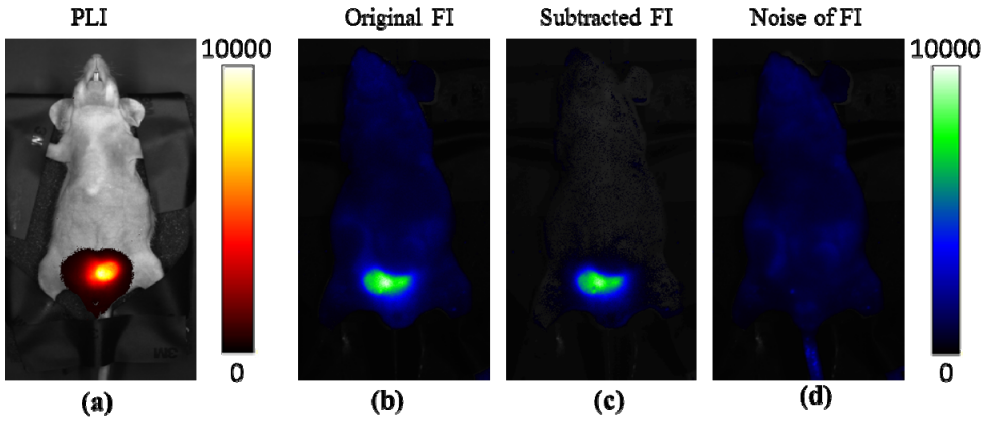

Fig. 7. Comparisons between PLI and FI for mouse experiments. (a) Fused PLI image with the white light image. (b) Fused original FI image with the white light image. (c) Fused subtracted FI image with the white light image. (d) Fused noise of FI image with the white light image.

Comparing with phantom experiment, the imaged object used in mouse experiment was changed into a mouse but with the similar target implant approach. So it was just an emulation to realistic biological application using realistic geometry and optical properties of a mouse in a real biological implementation. Besides that, noise of FI image for phantom experiment mainly contains bleed-through of excitation light, while mouse experiment mainly contains autofluorescence. PLI can completely circumvent the strong autofluorescence as shown in Fig. 7(a), but autofluorescence is distributed all over the body of the nude mouse in the noise of FI image (Fig. 7(d)), wihich has a significant interference to original FI image (Fig. 7(b)).

Biomedical Optics EXPRESS

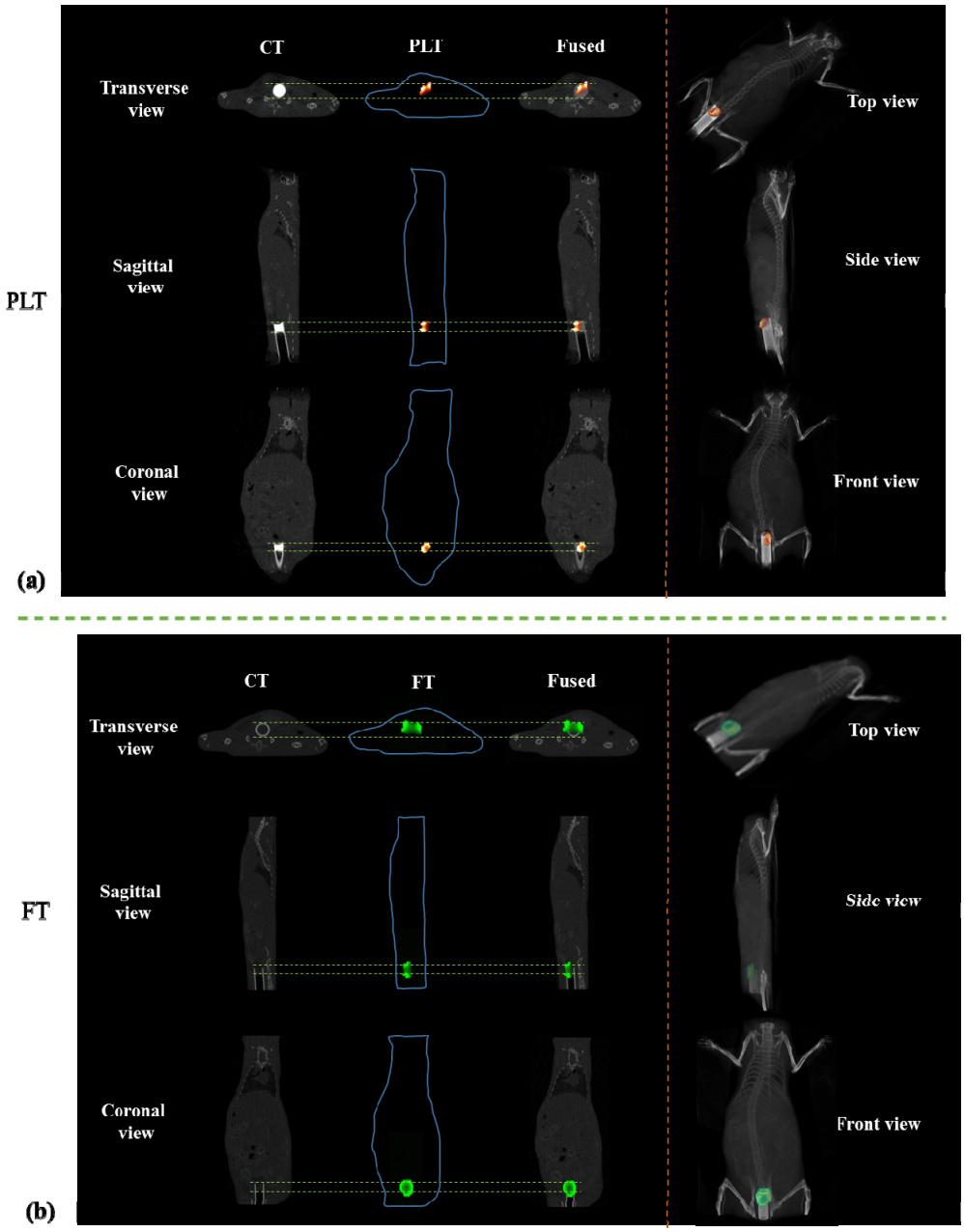

Fig. 8. Reconstructed results for the mouse experiment. (a) 2D sections (left) and 3D renderings (right) fused with the CT images for PLT. (b) 2D sections (left) and 3D volume renderings (right) fused with the CT images for FT.

Results of the mouse experiment are summarized in Fig. 8. Both reconstructed targets in 2D sections and 3D volume renderings for PLT and FT reconstructions are well conformed with those in CT images. But the size of the reconstructed FI target is slightly larger than that of the true one in the CT image. Quantitative analysis is listed in Table 2, and DIC of 0.66 and position error of 0.88 mm for PLT.

Biomedical Optics EXPRESS

Table 2. Quantitative analysis for PLT and FT reconstructions of the mouse experiment.

	DIC	True position	Reconstructed position	Position error
PLT	0.66	(31.76, 15.97,18.00)	(31.06, 15.67, 18.45)	0.88
FT	0.39	(30.67, 13.02, 10.78)	(30.46, 12.01, 11.54)	1.28

4. Conclusion

In this work, a tomographic imaging based on PL phenomenon termed as PLT was proposed. Although PLI has been used for *in vivo* applications in previous research [5, 6], it only focused on 2D imaging without depth information about PL probes. This work is the first time we know the feasibility of PLT to resolve the distributions of PL probes deep in turbid media and biological tissues.

After simplification, the forward model and reconstruction method for PLT are the same as BLT. But it is important to note that PLT has several advantages in biological applications. First, there are many usable PL probes for PLT to study different biological processes, but only the luciferase gene report system is usable for BLT. Second, BLT needs a complex transgene technique to construct animal models with cells marked with the luciferase gene. While PLT is a much easier tool, which just needs suitable PL probes injected into the tail vein like FI. Third, PLT is more flexible than BLT. The signals of BLT last just several minutes, which need to finish imaging in a short time window before the bioluminescence signals disappear. But signals of PLT can be produced using external excitation at any time before PL probes been metabolized, which may undergo several hours determined by the characteristics of the special PL probes.

Without interfering from tissue autofluorescence and bleed-through of excitation light, in-vitro results demonstrated that PLI had higher resolution than that of FI in signal acquisition, which implies PLT can provide a high sensitive and deep imaging in practical applications. But from the reconstructed results of the phantom and mouse experiments, it seems a slight improvement in PLT. That is because the PL and FI targets are artificial, which have high concentrations. In practical applications, PL and FI targets are formed by convergence in the lesion areas based on the specificities of themselves. Generally, convergence rates for PL and FI probes are not high enough to provide excellent SNR. So FI signals may be flooded in tissue autofluorescence and external excitation light, but PL signals do not have this problem.

Finally, it is believed that PLT will provide more potential in preclinical applications due to many PL probes produced by researchers. To improve the image quality of PLT, multi-projection acquisition is useful such as FMT.

Funding

This work was supported by the Program of National Natural Science Foundation of China under Grant Nos. 81227901, 61405149, 81230033, 61471279, 81530058, the Program of the National key Research and Development Program of China under Grant No. 2016YFC1300302, the Beijing Municipal Natural Science Foundation under Grant No. 7142012, the Natural Science Basic Research Plan in Shaanxi Province of China under Grant No. 2015JZ019, and the Fundamental Research Funds for the Central Universities NSIZ021402.